JOURNAL OF COMPUTATIONAL PHYSICS **139,** 359–379 (1998)
ARTICLE NO. CP975875

A Divergence-Free Multidomain Spectral Solver of the Navier–Stokes Equations in Geometries of High Aspect Ratio

C. Sabbah and R. Pasquetti

Laboratoire J.A. Dieudonné, UMR CNRS N° 6621, Université de Nice Sophia-Antipolis, Parc Valrose, Nice Cedex 2, 06108, France
E-mail: rpas@math. unice.fr

Received February 3, 1997; revised September 25, 1997

In order to solve with high accuracy the incompressible Navier-Stokes equations in geometries of high aspect ratio, one has developed a spectral multidomain algorithm, well adapted to the parallel computing. In cases of 2D problems, a Chebyshev collocation method and an extended influence matrix-technique are used in each subdomain, to solve the generalized Stokes problem which results from the discretization in time. The continuity conditions, needed at the interfaces of each subdomain, are computed by using again an influence matrix, the setup of which ensures all the necessary compatibility conditions, especially the incompressibility. This work is also described for 3D problems with one homogeneous direction. A study of accuracy versus the number of subdomains is presented, as well as an example of an application concerned with Rayleigh–Bénard convection in a cavity of large aspect ratio.

1. INTRODUCTION

Some physical problems require the accurate solution of the incompressible Navier–Stokes equations in geometries of high aspect ratio. As a matter of example, double diffusive convection in a tank of great height can be affected with instabilities that do not occur if the height is not large enough. Another problem of interest that requires such kinds of geometries is the study of the spatial development of wakes behind an obstacle. To this aim, we first developed a 2D Chebyshev multidomain parallel solver and this work was extended to the treatment of 3D geometries with one homogeneous direction. The multidomain approach is implemented along the direction of great length.

As it is well known, many approaches are possible for the approximation of the Navier–Stokes equations. Especially, one can use the so-called *projection* methods, as e.g. described in [1–4], or the two steps method described in [5], when restricting ourselves to the

0021-9991/98 $25.00

Chebyshev (or Legendre) spectral methods. Nevertheless, such approaches are often used to bypass the so-called generalized Stokes problem (GSP) which naturally results from the unsteady Stokes or Navier–Stokes equations, when using in time a finite difference scheme treating more or less implicitly the linear diffusion term and explicitly the nonlinear one, as generally done with spectral methods. Indeed, in nonperiodic geometries, solving the GSP is not a trivial task. Especially, approaches based on the direct solution of the so-called Uzawa operator to compute the pressure are generally not realistic, owing to memory storage requirements. This is the reason why iterative procedures are usually preferred, as e.g. in [6, 7], but the obtention of a satisfactory convergence rate is not straightforward.The monodomain GSP solver used in this work is briefly described in Section 2. It makes use of a spectral collocation method (see, e.g. [8]) based on an "extended influence matrix" technique, yielding the pressure, as well as the collocation error at the boundary, as first described in [9, 10]. The main advantage of such an approach is the obtention of the exact solution of the discrete form of the GSP, when its main drawback lays in its memory storage requirement. Moreover, owing to the use of the same grids and same polynomial vector spaces for the approximations of the velocity components and of the pressure, the latter is affected with spurious modes, as e.g. mentioned in [11]. For this reason, we also describe in Section 2 an algorithm to recover (when necessary) the pressure in a satisfactory way.

The multidomain procedure is considered is Section 3. Essentially, it is a nonoverlapping, patching, and direct method (based on an influence matrix technique) that is used for the computation of the velocity at the interfaces of the subdomains [8]. Once knowing the velocity at the boundary of each subdomain, one uses the monodomain GSP solver in each and finally derives the complete velocity field. As usual with patching methods, the continuity of the velocity at the interfaces is enforced strongly, as e.g. in [12] or in [13] (where an overlapping procedure is used). Such patching approaches differ from the variational approaches which generally only require the C^0 continuity of the velocity (see, e.g. [14, 15]). The method is direct, since it uses an influence matrix technique to compute the interface values (as in [12], where only one direction is nonhomogeneous). Such direct approaches are very efficient, but clearly require a sufficiently small number of interface collocation points. In other contexts, iterative procedures become necessary (as, e.g. in [16, 14]). In the framework of the vorticity-stream function formulation of the 2D Navier–Stokes equations, the use of an influence matrix technique is also suggested in [17–19]. But when using the velocity–pressure formulation the setup of this matrix is more complex, owing to the incompressibility constraint. In our approach compatibility conditions must be considered to preserve the main property of the monodomain solver, the divergence-free feature of the computed velocity. The approach makes intensive use of this property and utilizes original bases for spanning the interface velocity components.

The last section of this paper presents numerical results obtained on a CRAY T3D (or T3E) supercomputer. First, a study of accuracy is done by considering a GSP for which an analytical solution is known. Then we show the results of the numerical experiments concerned with 2D and 3D Rayleigh–Bénard convection in a cavity of aspect ratio equal to 8.

2. MONODOMAIN ALGORITHM

Let us consider the incompressible Navier–Stokes equations in a rectangular domain Ω of boundary Γ and assume admissible Dirichlet boundary conditions for the velocity. When

using in time an implicit (or semi-implicit) approximation of the diffusion term and an explicit one for the convection term, at each time step the GSP

$$\Delta \boldsymbol{V} - \sigma \boldsymbol{V} = \nabla p + \boldsymbol{f} \quad \text{in } \Omega \tag{1}$$

$$\nabla \cdot \boldsymbol{V} = 0 \quad \text{in } \bar{\Omega} \tag{2}$$

$$\boldsymbol{V}|_\Gamma = \boldsymbol{V}_\Gamma \tag{3}$$

has to be solved, with $\bar{\Omega}$ for the closure of Ω and where $\boldsymbol{V}$ stands for the velocity, p is for the pressure times the Reynolds number, and $\boldsymbol{f}$ is for a given body force term. The parameter σ is proportional to the ratio of the Reynolds number to the time step and depends on the scheme used for the discretization.

2.1. *"Extended Influence Matrix" Technique*

As is well known, as soon as the pressure and the body-force term are smooth enough, the problem (1)–(3) is equivalent to

$$\Delta \boldsymbol{V} - \sigma \boldsymbol{V} = \nabla p + \boldsymbol{f} \quad \text{in } \Omega \tag{4}$$

$$\Delta p + \nabla \cdot \boldsymbol{f} = 0 \quad \text{in } \Omega \tag{5}$$

$$\nabla \cdot \boldsymbol{V}|_\Gamma = 0 \tag{6}$$

$$\boldsymbol{V}|_\Gamma = \boldsymbol{V}_\Gamma. \tag{7}$$

Then the difficulty comes from the fact that no boundary conditions are available for the pressure. But this difficulty can be overcome by splitting the problem (4)–(7) into two problems [20],

$$\Delta \boldsymbol{V}^1 - \sigma \boldsymbol{V}^1 = \nabla p^1 + \boldsymbol{f} \quad \text{in } \Omega \tag{8}$$

$$\Delta p^1 + \nabla \cdot \boldsymbol{f} = 0 \quad \text{in } \Omega \tag{9}$$

$$p^1|_\Gamma = 0 \tag{10}$$

$$\boldsymbol{V}^1|_\Gamma = \boldsymbol{V}_\Gamma \tag{11}$$

and

$$\Delta \boldsymbol{V}^2 - \sigma \boldsymbol{V}^2 = \nabla p^2 \quad \text{in } \Omega \tag{12}$$

$$\Delta p^2 = 0 \quad \text{in } \Omega \tag{13}$$

$$p^2|_\Gamma = \mathcal{M}^{-1}\left(-\nabla \cdot \boldsymbol{V}^1|_\Gamma\right) \tag{14}$$

$$\boldsymbol{V}^2|_\Gamma = 0 \tag{15}$$

where $\mathcal{M}$ is an "influence operator" defined by

$$\mathcal{M} p^2|_\Gamma = \nabla \cdot V^2|_\Gamma \tag{16}$$

in such a way that

$$\nabla \cdot \boldsymbol{V}^1|_\Gamma + \nabla \cdot \boldsymbol{V}^2|_\Gamma = \nabla \cdot \boldsymbol{V}|_\Gamma = 0. \tag{17}$$

In Eq. (14) $\mathcal{M}^{-1}$ is a generalized inverse of the operator $\mathcal{M}$, since the pressure can only be defined up to a constant. After discretization, the operator $\mathcal{M}$ is the so-called influence matrix. It is built during a preliminary calculation, by solving a set of elementary problems similar to the problem (12)–(15), but with $p^2|_\Gamma$ given. Thus, when using a collocation method, the boundary values of p^2 are successively taken as unitary at the different boundary nodes to constitute the different columns of the influence matrix.

Such a splitting approach partially fails in the sense that the resulting velocity field is not perfectly divergence-free. Since [9, 10] this failure is well understood, the momentum equation (4) being not collocated at the boundary, the body force term of the Poisson equation (5) is polluted by an extra term that prevents from obtaining the desired result. Moreover, as shown in [10], where the tau method (see, e.g. [8]) is also investigated, this failure is not specific to the collocation method.

In order to outline this point and to briefly present the "extended influence matrix technique" (see [21] for an extensive presentation), let us assume that $\Omega =]-1, 1[^2$ (using a mapping if necessary) and introduce the $(I+1) \times (J+1)$ Gauss–Lobatto mesh associated with the Chebyshev polynomials:

$$\bar{\Omega}_{I,J} = \left\{ \cos\left(\frac{\pi i}{I}\right), \cos\left(\frac{\pi j}{J}\right) \right\}, \quad 0 \le i \le I; 0 \le j \le J, \tag{18}$$

$$\Omega_{I,J} = \left\{ \cos\left(\frac{\pi i}{I}\right), \cos\left(\frac{\pi j}{J}\right) \right\}, \quad 0 < i < I; 0 < j < J, \tag{19}$$

$$\Gamma_{I,J} = \bar{\Omega}_{I,J} \backslash \Omega_{I,J}. \tag{20}$$

Then, with $P_{I,J}$ the vector space of the polynomials of maximum degree I in x and J in y, the Chebyshev collocation method consists in finding $\boldsymbol{V}$ in $(P_{I,J})^2$ and p in $P_{I,J}$ such as

$$\Delta \boldsymbol{V} - \sigma \boldsymbol{V} = \nabla p + \boldsymbol{f} \quad \text{in } \Omega_{I,J} \tag{21}$$

$$\nabla \cdot \boldsymbol{V} = 0 \qquad \text{in } \bar{\Omega}_{I,J} \tag{22}$$

$$\boldsymbol{V}|_{\Gamma_{I,J}} = \boldsymbol{V}_{\Gamma_{I,J}}. \tag{23}$$

Here we notice that Eq. (22) implies that $\boldsymbol{V}$ is perfectly divergence-free, since a polynomial in $P_{I,J}$ which vanishes at $(I+1)(J+1)$ collocation points is the null polynomial. Moreover, the boundary condition (23) is assumed admissible; i.e, the polynomial interpolants of $\boldsymbol{V}_\Gamma|_{\Gamma_{I,J}}$ at each side of $\bar{\Omega}$ are compatible with the incompressibility constraint.

In order to take into account the error that occurs in the momentum equation, let us now introduce an additive unknown term $\boldsymbol{\tau}$, in $(P_{I,J})^2$ such that

$$\boldsymbol{\tau} = \boldsymbol{0} \quad \text{in } \Omega_{I,J} \tag{24}$$

and rewrite the following new version of system (4)–(7):

$$\Delta \boldsymbol{V} - \sigma \boldsymbol{V} = \nabla p + \boldsymbol{f} + \boldsymbol{\tau} \quad \text{in } \bar{\Omega}_{I,J} \tag{25}$$

$$\Delta p + \nabla \cdot \boldsymbol{f} + \nabla \cdot \boldsymbol{\tau} = 0 \quad \text{in } \Omega_{I,J} \tag{26}$$

$$\nabla \cdot \boldsymbol{V}|_{\Gamma_{I,J}} = 0 \tag{27}$$

$$\boldsymbol{V}|_{\Gamma_{I,J}} = \boldsymbol{V}_{\Gamma_{I,J}}. \tag{28}$$

The "extended influence matrix" algorithm is based on the splitting of problem (25)–(28),

$$\Delta \boldsymbol{V}^1 - \sigma \boldsymbol{V}^1 = \nabla p^1 + \boldsymbol{f} + \boldsymbol{\tau}^1 \quad \text{in } \bar{\Omega}_{I,J} \tag{29}$$

$$\Delta p^1 + \Delta \cdot \boldsymbol{f} = 0 \quad \text{in } \Omega_{I,J} \tag{30}$$

$$p^1|_{\Gamma_{I,J}} = 0 \tag{31}$$

$$\boldsymbol{V}^1|_{\Gamma_{I,J}} = \boldsymbol{V}_{\Gamma_{I,J}} \tag{32}$$

and

$$\Delta \boldsymbol{V}^2 - \sigma \boldsymbol{V}^2 = \nabla p^2 + \boldsymbol{\tau} + \boldsymbol{\tau}^2 \quad \text{in } \bar{\Omega}_{I,J} \tag{33}$$

$$\Delta p^2 + \nabla \cdot \boldsymbol{\tau} = 0 \quad \text{in } \Omega_{I,J} \tag{34}$$

$$\{p^2|_{\Gamma_{I,J}}, \boldsymbol{\tau}|_{\Gamma_{I,J}}\} = \mathcal{M}^{-1}\{-\nabla \cdot \boldsymbol{V}^1|_{\Gamma_{I,J}}, -\boldsymbol{\tau}^1|_{\Gamma_{I,J}}\} \tag{35}$$

$$\boldsymbol{V}^2|_{\Gamma_{I,J}} = 0, \tag{36}$$

where $\boldsymbol{\tau}^1$ and $\boldsymbol{\tau}^2$ are the collocation errors which occur at the boundary nodes, where the momentum equations are not enforced (N.B., $\boldsymbol{\tau}^1$ and $\boldsymbol{\tau}^2$ can only be computed *a posteriori*). $\mathcal{M}$ is now an influence matrix (and $\mathcal{M}^{-1}$ is a generalized inverse) defined by

$$\mathcal{M}\{p^2|_{\Gamma_{I,J}}, \boldsymbol{\tau}|_{\Gamma_{I,J}}\} = \{\nabla \cdot \boldsymbol{V}^2|_{\Gamma_{I,J}}, \boldsymbol{\tau}^2|_{\Gamma_{I,J}}\} \tag{37}$$

in such a way that

$$\nabla \cdot \boldsymbol{V}^1|_{\Gamma_{I,J}} + \nabla \cdot \boldsymbol{V}^2|_{\Gamma_{I,J}} = \nabla \cdot \boldsymbol{V}|_{\Gamma_{I,J}} = 0 \tag{38}$$

$$\boldsymbol{\tau}^1|_{\Gamma_{I,J}} + \boldsymbol{\tau}^2|_{\Gamma_{I,J}} = \boldsymbol{0}. \tag{39}$$

As presented here the dimension of the influence matrix $\mathcal{M}$ appears to be very large. But, in fact, this dimension can be drastically decreased because it is only the normal component of $\boldsymbol{\tau}$ that is required to compute $\nabla \cdot \boldsymbol{\tau}$ in $\Omega_{I,J}$. If we denote by τ the normal componant (to the boundary) of $\boldsymbol{\tau}$ and if we consider that $p^2|_{\Gamma_{I,J}} = p|_{\Gamma_{I,J}}$, then the influence matrix effectively involved in the computation is such that

$$\mathcal{M}\{p|_{\Gamma_{I,J}}, \tau|_{\Gamma_{I,J}}\} = \{\nabla \cdot \boldsymbol{V}^2|_{\Gamma_{I,J}}, \tau^2|_{\Gamma_{I,J}}\}. \tag{40}$$

Moreover, the collocation method does not need the values of p and τ at the four corners of the domain and so it only needs these values at $2(I + J - 2)$ boundary nodes. The

dimension of the extended influence matrix is then $4(I + J - 2)$, i.e. twice larger than the usual influence matrix. It can be set up in a preliminary calculation by solving the elementary problems associated with the canonical basis of the vector space $R^{4(I+J-2)}$ for the boundary node values of p^2 and τ in Eqs. (33) and (34). Once the influence matrix is calculated, one has to invert it, but as outlined later in the text one has a rank deficiency equal to four. One way to proceed is to compute the eigenvalues and then replace the four zero values by nonnull values, in order to project the solution onto the orthogonal complement of the kernel. Contrary to what is mentioned in [22], where one suggests using infinite values, the nonnull values can be arbitrary, without any incidence on $p|_{\Gamma_{I,J}}$ and $\tau|_{\Gamma_{I,J}}$.

Finally, the algorithm is the following:

—solve the problem (29)–(32) and, once knowing the velocity and pressure fields $\boldsymbol{V}^1$ and p^1, compute the values of $\nabla \cdot \boldsymbol{V}^1|_{\Gamma_{I,J}}$ and $\tau^1|_{\Gamma_{I,J}}$;

—from Eq. (35) compute the boundary values of the pressure $p|_{\Gamma_{I,J}}$ and of the correction term $\tau|_{\Gamma_{I,J}}$;

—solve the problem (25)–(28) using the prescribed values of $p|_{\Gamma_{I,J}}$ and $\tau|_{\Gamma_{I,J}}$.

Remark. The initial problem (21)–(23) only requires the knowledge of $\boldsymbol{f}$ in $\Omega_{I,J}$, on the contrary of the approach, based on the standard influence matrix technique. This property is recovered when using the extended influence matrix approach, since the error term τ permits us to assume arbitrary values of $\boldsymbol{f}$ at the the boundary nodes. Thus, one can simply assume $\boldsymbol{f}|_{\Gamma_{I,J}} = \boldsymbol{0}$.

2.2. *Calculation of the Pressure*

The advantage of assuming p in $P_{I,J}$ is that a divergence-free velocity field $\boldsymbol{V}$ can effectively be produced, but this advantage goes with the drawback that the pressure is affected with spurious modes [23]. With $T_i(x) = \cos i(\cos^{-1} x)$ for the Chebyshev polynomial of degree i, these spurious modes are:

—the constant mode $T_0(x)T_0(y) = 1$, which is physical, since the pressure is defined up to a constant,
—the column mode $T_I(x)T_0(y) = T_I(x)$,
—the line mode $T_0(x)T_J(y) = T_J(y)$,
—the checkerboard mode $T_I(x)T_J(y)$.

The nonphysical spurious modes result from the definition of the Gauss–Lobatto mesh (Eq. (18)) for which $(1-x^2)(1-y^2)T_I'(x)T_J'(y) = 0$ (with a prime for the first-order derivative). Moreover, since the corner values of the pressure are not required by the algorithm so they can be arbitrary, one has also:

—the four corner modes.

In the framework of the "extended influence matrix technique" the spurious modes of pressure are associated with spurious modes of $\boldsymbol{\tau}$. Indeed, from Eqs. (25) and (26), it is clear that the spurious parts p_{sp} and $\boldsymbol{\tau}_{sp}$ of p and $\boldsymbol{\tau}$ verify the set of equations [22]:

$$\nabla p_{sp} + \boldsymbol{\tau}_{sp} = \boldsymbol{0} \quad \text{in } \bar{\Omega}_{I,J} \tag{41}$$

$$\boldsymbol{\tau}_{sp}|_{\Omega_{I,J}} = \boldsymbol{0} \tag{42}$$

$$\Delta p_{sp} + \nabla \cdot \boldsymbol{\tau}_{sp} = 0 \quad \text{in } \Omega_{I,J}. \tag{43}$$

Then,

$$
\begin{aligned}
&-\boldsymbol{\tau}_{sp} = (0, 0),\\
&-\boldsymbol{\tau}_{sp} = (-T_I'(x), 0),\\
&-\boldsymbol{\tau}_{sp} = (0, -T_J'(y)), \text{ and}\\
&-\boldsymbol{\tau}_{sp} = (-T_I'(x)T_J(y), -T_I(x)T_J'(y))
\end{aligned}
$$

are respectively associated with the constant, column, line, and checkerboard modes. The restictions to the boundary of these four spurious couples constitute a basis of the influence matrix kernel. Consequently, $\mathcal{M}$ has a rank deficiency equal to four, as mentioned in Section 2.1.

Remark. When using the standard influence matrix approach, the Poisson equation (43) for p_{sp} becomes homogeneous and is no longer verified by the nonphysical spurious modes. The dimension of the kernel of the standard influence matrix then equals one.

How can we recover the pressure field? The natural idea is to filter the nonphysical modes, but more problematic is the question of the corner modes, since vanishing the pressure at the four corners of the domain is clearly not physical. Let us first assume that the values $p_l, 1 \leq l \leq 4$, of the pressure at the corners are known. Then, in the Chebyshev spectral space the spurious modes can be cancelled, in order to get the filtered pressure field p', which depends on the p_l. The natural idea is then to produce a smooth pressure field. This can be achieved by solving the following optimization problem: find the p_l such that the functional

$$J(p_l) = \sum_{\bar{\Omega}_{I,J}} |\nabla p'|^2 \tag{44}$$

is minimal. But in $\Omega_{I,J}$ the gradient of the pressure does not depend on the pressure spurious modes, so that the functional can be rewritten in the simpler form,

$$J(p_l) = \sum_{\Gamma_{I,J}} |\nabla p'|^2. \tag{45}$$

This optimization problem can be easily solved after noticing that p can read

$$p = p_0 + \sum_l p_l C_l, \tag{46}$$

where p_0 is the initial pressure field with zero values at the corners and where the C_l are the polynomials which vanish everywhere in $\bar{\Omega}_{I,J}$, except at the corners where they take unitary values. After filtering the four spurious modes one gets

$$p' = p_0' + \sum_l p_l C_l', \tag{47}$$

$$\nabla p' = \nabla p_0' + \sum_l p_l \nabla C_l', \tag{48}$$

where the $\nabla C_l'$ vanish in $\Omega_{I,J}$. It is then easy to express $\nabla p'|_{\Gamma_{I,J}}$ in terms of the p_l and to compute these p_l by using a standard least square method.

2.3. *Extension to 3D Geometries with One Homogeneous Direction*

When assuming that the z direction is homogeneous a discrete Fourier expansion of the different variables can be used along this direction. Then, the 3D problem decouples into a set of 2D complex problems. Namely, for each mode number $k, 0 \leq k \leq K$, one gets the following system of equations that must solve the Fourier spectra (denoted by $\hat{.}_k$) of the different variables,

$$\Delta_k \hat{\boldsymbol{V}}_k - \sigma \hat{\boldsymbol{V}}_k = \nabla_k \hat{p}_k + \hat{\boldsymbol{f}}_k + \hat{\boldsymbol{\tau}}_k \quad \text{in } \bar{\Omega}_{I,J} \tag{49}$$

$$\Delta_k \hat{p}_k + \nabla_k \cdot \hat{\boldsymbol{f}}_k + \nabla_k \cdot \hat{\boldsymbol{\tau}}_k = 0 \tag{50}$$

$$\nabla_k \cdot \hat{\boldsymbol{V}}_k|_{\Gamma_{I,J}} = 0 \tag{51}$$

$$\hat{\boldsymbol{V}}_k|_{\Gamma_{I,J}} = \hat{\boldsymbol{V}}_{k\Gamma_{I,J}}, \tag{52}$$

where $\Delta_k = \partial_{xx} + \partial_{yy} - k^2$ and $\nabla_k = (\partial_x, \partial_y, \mathrm{i}k)$, with i for the square root of -1. For each mode number one can apply the extended influence matrix algorithm and thus obtain a set of influence matrices $\mathcal{M}_k$, such that

$$\mathcal{M}_k\{\hat{p}_k|_{\Gamma_{I,J}}, \hat{\tau}_k|_{\Gamma_{I,J}}\} = \left\{\nabla_k \cdot \hat{\mathbf{V}}_k^2|_{\Gamma_{I,J}}, \hat{\tau}_k^2|_{\Gamma_{I,J}}\right\}. \tag{53}$$

These influence matrices $\mathcal{M}_k$ are real; they associate the real (imaginary) parts of $\{\hat{p}_k|_{\Gamma_{I,J}}, \hat{\tau}_k|_{\Gamma_{I,J}}\}$ to the real (imaginary) parts of $\{\nabla_k \cdot \hat{\boldsymbol{V}}_k^2|_{\Gamma_{I,J}}, \hat{\tau}_k^2|_{\Gamma_{I,J}}\}$.

Finally, one has to mention that for $k \neq 0$, the influence matrices are regular. This results from the fact that if $\hat{p}_k$ does not vanish in $\Omega_{I,J}$, then $\nabla_k \hat{p}_k$ is also nonnull in $\Omega_{I,J}$. On the contrary, if $k = 0$ the 2D situation and the spurious modes of pressure are recovered.

3. MULTIDOMAIN APPROACH

In this section we present a multidomain approach, based on the use of the monodomain solver which has just been presented, to solve the GSP with the no-slip boundary condition. First we begin with the 2D case, by considering for the domain Ω a rectangle of large aspect ratio. This domain Ω is splitted, versus the direction of great length (x direction) into a set of N subdomains Ω_n. The interface between the subdomains Ω_n and Ω_{n+1} is denoted by I_n. At the intersections of I_n and of the boundary Γ of Ω, one has the points A_n and B_n in such a way that Ω_n, of boundary Γ_n, is the square A_{n-1}, A_n, B_n, B_{n-1}. Moreover we assume the use of matching grids: for all n, the number of collocation points between the points A_n and B_n is equal to $(J-1)$.

3.1. *Interface Conditions*

With $\boldsymbol{V} = (u, v)$ and $[\![\cdot]\!]_n$ for the jump at the interfaces I_n, the essential and natural continuity conditions that the PDE (1) induces to use at these interfaces read:

$$[\![u]\!]_n = [\![v]\!]_n = [\![\partial_x u - p]\!]_n = [\![\partial_x v]\!]_n = 0. \tag{54}$$

Nevertheless, when taking into account that the velocity is divergence-free, the first, second, and fourth conditions imply that u is C^2-continuous:

$$[\![\partial_x u]\!]_n + [\![\partial_y v]\!]_n = [\![\partial_x u]\!]_n = 0 \tag{55}$$

$$[\![\partial_{xx} u]\!]_n + [\![\partial_{xy} v]\!]_n = [\![\partial_{xx} u]\!]_n = 0. \tag{56}$$

It results that in the case of incompressible fluids the interface conditions read:

$$[\![u]\!]_n = [\![v]\!]_n = [\![p]\!]_n = [\![\partial_x v]\!]_n = 0. \tag{57}$$

Let us go to the discrete framework. When using the approach described in Section 2, the previous interface conditions should still hold, because the approximate velocity field is also perfectly divergence-free. But the spurious modes of pressure prevent the use of the third condition, i.e. the one involving the pressure jump.

In order to overcome this difficulty, we first tried to enforce the C^2 continuity of v rather than the C^0 continuity of p, i.e. to substitute for the condition $[\![p]\!]_n = 0$ the one, $[\![\partial_{xx} v]\!]_n = 0$. Such an approach is quite satisfactory for solving a GSP and even the nonstationary Navier–Stokes equations at low Reynolds numbers. Unfortunately, when the Reynolds number is increased, oscillations of the solution generally occur at the interfaces I_n and then amplify, until inducing numerical instability.

The way that we suggest and use now successfully, consists in a weak formulation of the interface condition $[\![p]\!]_n = 0$. This permits us to overcome efficiently the problem of the spurious modes of pressure, without inducing any deterioration of the solution at the interfaces I_n. For the sake of clarity, this weak formulation of the pressure continuity condition will be detailed in Subsection 3.3, after the description of the influence matrix technique that is used in our multidomain approach.

Remark. The interface conditions (57) induce the C^0 continuity of the vorticity, $\omega = \partial_x v - \partial_y u$.

3.2. *Influence Matrix Technique*

Let us split the GSP into two sets of N monodomain problems, P_n^1 and P_n^2. For the first set, one assumes for each subdomain homogeneous Dirichlet boundary conditions and one takes into account the body-force term:

Problems P_n^1 read:

$$\Delta \boldsymbol{V}^1 - \sigma \boldsymbol{V}^1 = \nabla p^1 + \boldsymbol{f} \quad \text{in } \Omega_n \tag{58}$$

$$\nabla \cdot \boldsymbol{V}^1 = 0 \qquad \text{in } \bar{\Omega}_n \tag{59}$$

$$\boldsymbol{V}^1|_{\Gamma_n} = 0. \tag{60}$$

Once this first set of problems is solved the jumps $[\![p^1]\!]_n$ and $[\![\partial_x v^1]\!]_n$ can be computed.

For the second set of problems, one uses at the interfaces I_n, $1 \le n \le (N-1)$, the nonhomogeneous Dirichlet conditions $(u^2, v^2)|_{I_n}$, which ensure the interface conditions, i.e. such that for all n,

$$[\![p^1]\!]_n + [\![p^2]\!]_n = 0 \tag{61}$$

$$[\![\partial_x v^1]\!]_n + [\![\partial_x v^2]\!]_n = 0. \tag{62}$$

Problems P_n^2 read:

$$\Delta \boldsymbol{V}^2 - \sigma \boldsymbol{V}^2 = \nabla p^2 \quad \text{in } \Omega_n \tag{63}$$

$$\nabla \cdot \boldsymbol{V}^2 = 0 \qquad \text{in } \bar{\Omega}_n \tag{64}$$

$$\boldsymbol{V}^2|_{\Gamma_n} = \boldsymbol{V}_{\Gamma_n}. \tag{65}$$

Then $\boldsymbol{V}^1 + \boldsymbol{V}^2$ is the solution of the complete problem.

Thanks again to the linearity property of the GSP, in order to determine the appropriate values of $(u^2, v^2)|_{I_n}$, in fact equal to $(u, v)|_{I_n}$, a new influence matrix M can be introduced such that

$$M\{\cup(u, v)|_{I_n}\} = \{\cup([\![p^2]\!]_n, [\![\partial_x v^2]\!]_n)\} \tag{66}$$

with $\cup$ for union over n $(1 \le n \le (N-1))$.

The influence matrix M is clearly block tridiagonal, since if the velocity is only nonnull at the interface I_n, then the jumps $[\![p]\!]_n$ and $[\![\partial_x v]\!]_n$ are only nonnull at the interfaces I_n, I_{n+1}, and I_{n-1} (when they exist). Three blocks (at most) are thus associated with the interface I_n. The aim is to set up these blocks, but such a task needs some attention as outlined now.

In the discrete framework, the couple $(u, v)|_{I_n}$ cannot take arbitrary values in $R^{2(J-1)}$, since constraints, especially coming from the incompressibility and compatibility conditions at the "corners" A_n and B_n, must be taken into account. This results in the fact that, to the contrary of what was done for the computation of the influence matrix $\mathcal{M}$, here one cannot simply solve elementary problems associated with the canonical basis of $R^{2(J-1)}$, since they would involve nonadmissible boundary conditions and so would be ill-posed. The elementary problems must now be associated with an appropriate basis, spanning the admissible values of (u, v) at the interface. The compatibility constraints result from the no-slip condition

$$u(A_n) = u(B_n) = v(A_n) = v(B_n) = 0 \tag{67}$$

and from the continuity equation

$$\partial_y v(A_n) = \partial_y v(B_n) = 0. \tag{68}$$

The constraints of incompressibility read:

$$\int_{I_n} u \, dy = 0, \tag{69}$$

$$u|_{I_n} \in P_{J-1}. \tag{70}$$

This last constraint results from the fact that the polynomials $\partial_x u$ and $\partial_y v$ must take their values in the same polynomial vector space, so that their sum can identically vanish. This vector space, at the intersection of $P_{I-1,J}$ and $P_{I,J-1}$, is $P_{I-1,J-1}$. It derives that actually $u \in P_{I,J-1}$ and that $v \in P_{I-1,J}$.

Let us first produce a basis for $u|_{I_n}$. When knowing that

$$T_j(\pm 1) = (\pm 1)^j \tag{71}$$

$$\int_{-1}^{1} T_j(y)\, dy = \frac{-2}{j^2-1}, \quad j \text{ even; 0 if } j \text{ is odd}, \tag{72}$$

one can introduce the set of $(J-3)$ polynomials $e_j(y)$ of degree j, such that $3 \le j \le J-1$:

1. j odd and $j \ge 3$,

$$e_j(y) = T_j(y) - T_1(y) \tag{73}$$

2. j even and $j \ge 4$,

$$e_j(y) = T_j(y) - \alpha T_2(y) - \beta, \tag{74}$$

where

$$\alpha = \frac{3j^2}{4(j^2-1)}, \quad \beta = \frac{j^2-4}{4(j^2-1)}. \tag{75}$$

The polynomials $e_j(y)$ verify the constraints (67), (69), and (70), are clearly nonlinearly dependent and their number $(J-3)$ equals the number of degrees of freedom $(J+1)$, decreased by the four constraints.

Let us now produce a basis for $v|_{I_n}$. With (71) and knowing that

$$T_j'(\pm 1) = j^2(\pm 1)^{j+1}, \tag{76}$$

the following set of $(J-3)$ polynomials of degree j, $4 \le j \le J$, is well suited:

1. j odd and $j \ge 5$,

$$e_j(y) = T_j(y) - \alpha T_1(y) - \beta T_3(y), \tag{77}$$

where

$$\alpha = \frac{9-j^2}{8}, \quad \beta = \frac{j^2-1}{8}; \tag{78}$$

2. j even and $j \ge 4$,

$$e_j(y) = T_j(y) - \alpha T_0(y) - \beta T_2(y), \tag{79}$$

where

$$\alpha = 1 - \frac{j^2}{4}, \quad \beta = \frac{j^2}{4}. \tag{80}$$

The polynomials $e_j(y)$ now verify the constraints (67) and (68) and constitute an appropriate basis for $v|_{I_n}$.

In order to compute the components of $u|_{I_n}$ and $v|_{I_n}$ in the bases that have just been defined, if appears that only $2(J-3)$ relations are prescribed from Eqs. (61) and (62). This may be surprising, since the number of collocation points between A_n and B_n is equal to $(J-1)$. Concerning the continuity of the pressure, it is shown in the next subsection that the weak formulation of the pressure jump only yields $(J-3)$ relations. Concerning the C^1 continuity of v, $(J-3)$ relations are only required, as explained below.

At the "corners" A_n and B_n one has the following compatibility conditions, resulting from the no-slip boundary condition and from the continuity equation:

$$\partial_{yx} v(A_n) = \partial_{yx} v(B_n) = 0. \tag{81}$$

These compatibility conditions permit us, in the discrete framework, to calculate the values of $\partial_x v$ at two collocation points, once we know their values at the $(J-3)$ other ones. It results that Eq. (62) has only to be expressed at $(J-3)$ collocation point. Thus, we do not consider the collocation points nearest to A_n and B_n. Consequently, the influence matrix M in Eq. (66) is square, each of its block being of dimension $2(J-3)$, and in this equation $(u, v)|_{I_n}$ must be viewed as the components of $u|_{I_n}$ and $v|_{I_n}$ in their specific bases.

3.3. *Weak Formulation of the Pressure Continuity Condition*

When restricted to an interface I_n, $[\![p]\!]_n$ is a polynomial in P_J, affected by the following spurious modes of pressure:

—$T_0(y) = 1$ (the constant physical mode)
—$T_J(y)$
—the A_n and B_n "corner" modes, i.e. the two polynomials which vanish at all the collocation points of the interface I_n, except at the points A_n and B_n, where they take unitary values.

Let us introduce the following weak formulation of the condition $[\![p]\!]_n = 0$:

1. j odd and $J > j \geq 3$,

$$\int_{I_n} [\![p]\!]_n (T_j(y) - T_1(y))\, d\mu = 0 \tag{82}$$

2. j even and $J > j \geq 4$,

$$\int_{I_n} [\![p]\!]_n (T_j(y) - T_2(y))\, d\mu = 0 \tag{83}$$

where

$$d\mu = (1 - y^2)^{-1/2} dy. \tag{84}$$

With such a measure the chebyshev polynomials are orthogonal. Consequently, the spurious part of $[\![p]\!]_n$ spanned by the polynomials $T_J(y)$ and $T_0(y)$ is cancelled. Moreover, the

weighting functions are also orthogonal to the pressure corner modes, because they vanish at points A_n and B_n from property (71). This can be checked from the Gauss–Lobatto quadrature formula, which is exact for polynomials of degree up to $(2J-1)$ (see, e.g. [23]).

Thus, formulas (82) and (83) constitute a set of $(J-3)$ equations expressing a weak formulation of the interface condition $[\![p]\!]_n = 0$ and got rid of the spurious modes of pressure (including the physical constant mode). From the Gauss–Lobatto quadrature formula, it reads

$$\sum_{m=1}^{J-1} [\![p]\!]_n(y_m)(T_j(y_m) - T_l(y_m)) = 0, \quad 3 \le j < J, \tag{85}$$

with $l=1$ if j is odd and $l=2$ if j is even. Knowing that $T_j(y_m) = \cos(\pi jm/J)$, this set of equations can be expressed in matrix form by introducing a matricial operator H of dimension $(J-3)\times(J-1)$, the elements of which can be easily identified as

$$H_{j-2,m} = \cos\left(\frac{\pi jm}{J}\right) - \cos\left(\frac{\pi lm}{J}\right), \tag{86}$$

where $3 \le j < J$ and $1 \le m \le J-1$.

3.4. *Extension to 3D Geometries with One Homogeneous Direction*

With $\hat{\boldsymbol{V}}_k = (\hat{u}_k, \hat{v}_k, \hat{w}_k)$, for the spectrum of $\boldsymbol{V}$, let us first consider the case $k=0$ which is very similar to the 2D situation.

If $k=0$, the operator ∇_k reads $\nabla_0 = (\partial_x, \partial_y, 0)$. Then, considering again the GSP, one observes that the equation for $\hat{w}_0$ is not coupled to the equations for $\hat{u}_0$ and $\hat{v}_0$. One can thus apply for $\hat{u}_0$ and $\hat{v}_0$ the approach used previously in the 2D situation and consider independently the variable $\hat{w}_0$ which solves an elliptic Helmholtz equation. In the multidomain context, the natural procedure is then to enforce the C^1 continuity at the interfaces. This is done by using a block tridiagonal influence matrix M_0' such that

$$M_0'\{\cup(\hat{w}_0)|_{I_n}\} = \left\{\cup\left([\![\partial_x \hat{w}_0^2]\!]_n\right)\right\}. \tag{87}$$

The different blocks of this influence matrix can be built easily in a preliminary calculation by solving for each interface I_n the elementary problems associated with the canonical basis of R^{J-1}. Then, one computes $\hat{w}_0$ in two steps: the first one considers in each subdomain homogeneous boundary conditions and the second one takes into account the values of $\hat{w}_0$ at the interfaces.

Remark. When an advection-diffusion equation is associated to the Navier–Stokes equations, e.g. for the temperature, at each time step one has to associate to the GSP an elliptic Helmhotz equation. This elliptic Helmholtz equation can be solved (for all mode numbers, in the 3D situation considered in this section) as it has just been described for $\hat{w}_0$.

Let us now consider the case $k \neq 0$, which is less staightforward. The interface conditions that must be enforced are the C^0 continuity of $\hat{u}_k$ and $\hat{p}_k$, without the requirement of a weak formulation, and the C^1 continuity of $\hat{v}_k$ and $\hat{w}_k$. But as in the 2D case, one can easily observe that the continuity equation induces that $\hat{u}_k$ is actually C^2 continuous. It derives that the vorticity vector and stress tensor spectra are C^0 continuous.

Thus, in 3D with one homogeneous direction, we are led to introduce influence matrices M_k, such that

$$M_k\{\cup(\hat{u}_k, \hat{v}_k, \mathrm{i}\hat{w}_k)|_{I_n}\} = \left\{\cup\left([\![\partial_x \hat{v}_k^2]\!]_n, [\![\partial_x \mathrm{i}\hat{w}_k^2]\!]_n, [\![\hat{p}_k^2]\!]_n\right)\right\}. \tag{88}$$

One notices that the variable $\mathrm{i}\hat{w}_k$ is used in such a way that all the operators of the GSP become real. Consequently, the matrices M_k are also real and the determinations of the real and imaginary parts of $\{\cup(\hat{u}_k, \hat{v}_k, \mathrm{i}\hat{w}_k)|_{I_n}\}$ are not coupled. As the matrix M (and M_0'), the matrices M_k are block tridiagonal, with three blocks associated with each interface I_n.

As in the 2D situation, the problem is now to set up these blocks, but no new difficulty arises and, on the contrary, one difficulty falls. Similarly to the 2D case (Eqs. (67) and (68)), one has some constraints which result from the no-slip condition, expressed at the corners,

$$\hat{u}_k(A_n) = \hat{u}_k(B_n) = \hat{v}_k(A_n) = \hat{v}_k(B_n) = \hat{w}_k(A_n) = \hat{w}_k(B_n) = 0, \tag{89}$$

and from the continuity equation,

$$\partial_y \hat{v}_k(A_n) = \partial_y \hat{v}_k(B_n) = 0. \tag{90}$$

But to the contrary of the 2D situation, the incompressibility constraints (69) and (70) no more exist, since

—the velocity fields associated with the mode numbers $k \neq 0$ automatically satisfy Eq. (69),

—in the spectrum of $\nabla \cdot \boldsymbol{V}$ the term $ik\hat{w}_k$ which is in $P_{I,J}$ now appears.

One observes that $\hat{u}_k|_{I_n}$ and $\hat{w}_k|_{I_n}$ are simply polynomials in P_J which vanish at points A_n and B_n. In this case using the basis (73), (74) is useless and one simply considers the elementary problems associated with the canonical basis of R^{J-1}. For $\hat{v}_k|_{I_n}$ the constraints are the same as the ones met in the 2D situation, so that the basis (77), (79) has to be used and in Eq. (88) $\hat{v}_k|_{I_n}$ must be viewed in this basis. On the other hand, similarly to Eq. (81) one has the compatibility conditions

$$\partial_{yx} \hat{v}_k(A_n) = \partial_{yx} \hat{v}_k(B_n) = 0 \tag{91}$$

which state that the collocation point values of $\partial_x \hat{v}_k$ can only be arbitrary at $J-3$ collocation points, so that the continuity of $\partial_x \hat{v}_k$ should not be imposed everywhere. We do not collocate these equations at the points nearest of the boundary. If results that the dimension of each block of influence matrices M_k is $(3J-5)$.

4. NUMERICAL TESTS

In order to check the capabilities of the present Stokes solver, two studies have been carried out. In the first one which considers the Stokes problem (1)–(3) in a cavity of aspect ratio equal to 16, our aim is to produce some quantitative results when varying the mesh refinement and the subdomain number. The second considers a Rayleigh–Bénard problem in a cavity of aspect ratio equal to 8.

4.1. *Stokes Solver Accuracy*

At first some analytical fields ($\boldsymbol{V}$, p) have to be produced. The results obtained from the Stokes solver will then be compared to them. The analytical velocity field must be divergence-free, null at the boundary, and homogeneous versus the z-axis. In order to support these constraints, in the domain $\Omega =]0, L_x[\times]0, 1[\times]0, L_z[$, let us introduce the vector:

$$\boldsymbol{\psi} = \psi(1, 1, 1), \tag{92}$$

where

$$\psi = Cx^2(x - L_x)^2y^2(y - 1)^2 \cos(11x)\cos(7y)\left(1 + \cos\left(6\frac{2\pi}{L_z}z\right)\right) \tag{93}$$

and define the velocity field $\boldsymbol{V}$ as the curl of $\boldsymbol{\psi}$: $\boldsymbol{V} = \nabla \times \boldsymbol{\psi}$. In (93) C is a normalization factor chosen to induce $\max(|\boldsymbol{V}|) \approx 1$.

Concerning the pressure, we assume:

$$p = 0.5\cos(7x)\cos(11y)\left(1 + \cos\left(3\frac{2\pi}{L_z}z\right)\right). \tag{94}$$

From the analytical forms of $\boldsymbol{V}$ and p and for a given value of the parameter σ, using the symbolic calculation (MAPLE software), the analytical expression of the body force term is derived (see Eqs. (1)–(3)).

All the calculations have been performed for the following set of the different parameters: $L_x = 16$, $L_z = 6$, $C = 1/7000$, $\sigma = 10^4$, and, concerning the mesh, $K = 8$, $J = \{8, 16, 32\}$, and $I = 16J$. In fact, the value $J = 8$ is too small to get satisfactory results, whereas $J = 32$ yields the machine accuracy for the velocity, except for the highest value $N = 32$ subdomains. Moreover, let us emphasize that in the Fourier spectral space only the mode numbers 0, 3, and 6 of the analytical solutions are different from zero, in such a way that for $K = 8$, the accuracy defaults can only result from the parameters J and N. The total number of collocation points is $2K(J + 1)(I + 1)$.

The numerical results are given in Tables 1 and 2, where the mean-quadratic and maximal errors are mentioned for the modulus of the velocity and for the pressure for different couples (J, N). (N.B., For the couples (2, 32) and (4, 32), the memory requirements were too large for the T3D processors.)

It is interesting to observe that the errors are slowy increasing with N until the number of collocations in each subdomain become too small. Indeed, with $J = 16$ and $N = 32$, there

TABLE 1
Mean-Quadratic and Maximal Errors for the Velocity Modulus

N	2	4	8	16	32
$J = 16$	1.39E-8	1.78E-8	2.03E-8	1.32E-7	1.36E-4
	4.88E-8	4.88E-8	4.88E-8	5.45E-7	4.58E-4
$J = 32$			6.06E-15	4.81E-15	3.42E-12
			2.13E-14	2.13E-14	1.43E-11

TABLE 2
Mean-Quadratic and Maximal Errors for the Pressure

N	2	4	8	16	32
$J=16$	1.65E-5	2.37E-5	2.82E-5	4.78E-4	0.44
	6.28E-5	6.76E-5	7.71E-5	1.34E-3	0.99
$J=32$			1.69E-7	6.01E-6	1.46E-5
			1.94E-7	6.87E-6	1.66E-5

are only nine points along the x axis in each subdomain. For smaller values of N, the error is essentially governed by the largest value of the x-space step, which does not depend on the number of subdomains.

One can also observe in Table 2 that the computation of the pressure is rather accurate and that the spurious mode-cleaning algorithm proposed in Section 2.2 is efficient. Nevertheless, with $J=16$ and $N=32$, the results on the pressure are no longer acceptable, whereas the results for the velocity are still reasonably satisfactory.

Remark 1. In some situations, the use of subdomains can improve the accuracy of the numerical results, especially, when a stiff gradient occurs between two subdomains or if a subdomain is affected to the approximation of a boundary layer [24]. Consequently, it can be interesting to match the subdomains with the expected solution.

Remark 2. When using for the mode number $k=0$ the interface condition $[\![\partial_{xx} v]\!]_n = 0$, rather than the weak formulation of $[\![p]\!]_n = 0$, one obtains results very similar to those of Tables 1 and 2 , as shown in Tables 3 and 4, respectively.

4.2. *Rayleigh–Bénard Convection*

The multidomain GSP solver described in this paper has been used for solving the Boussinesq–Oberbeck equations in a 3D cavity such as $L_x=8$ and $L_z=2.8$, the gravity being parallel to the y direction. The Rayleigh number is taken $\mathrm{Ra}=3000$ and the Prandtl number is the air's, $\mathrm{Pr}=0.71$. The boundary and initial conditions are defined below.

Boundary conditions. For the velocity we assume the no-slip boundary condition. For the temperature, we assume Dirichlet conditions at the bottom and at the top of the cavity, $T=1$ and $T=0$, respectively, in nondimensional form and homogeneous Neumann conditions (adiabaticity condition) at the lateral walls.

TABLE 3
Mean-Quadratic and Maximal Errors for the Velocity Modulus

N	2	4	8	16	32
$J=16$	1.39E-8	1.78E-8	2.03E-8	3.65E-7	5.83E-3
	4.88E-8	4.88E-8	4.88E-8	1.43E-6	3.56E-2
$J=32$			9.20E-14	4.50E-14	1.51E-11
			2.37E-13	1.55E-13	3.60E-11

TABLE 4
Mean-Quadratic and Maximal Errors for the Pressure

N	2	4	8	16	32
$J=16$	1.65E-5	2.37E-5	2.82E-5	8.80E-4	0.66
	6.28E-5	6.76E-5	7.71E-5	2.58E-3	1.62
$J=32$			1.69E-7	6.01E-6	1.46E-5
			1.94E-7	6.87E-6	1.66E-5

Initial conditions. The fluid is assumed to be at rest. The temperature is in the conductive state, i.e. linearly variable from the bottom to the top of the cavity. But to induce a 3D flow, this temperature profile is perturbated with the function

$$\epsilon = -10^{-3}\sin(\pi y)\cos\left(\frac{\pi}{0.8}\left(x+\cos\left(\frac{\pi}{1.4}z\right)\right)\right). \tag{95}$$

Such a perturbation, which is periodic in z and which vanishes at the top and at the bottom of the cavity, induces in the box $]0, 8[\times]0, 1[\times]0, 2.8[$ a set of 10 rolls, the axis of which are distorted following a sinusoïdal variation of amplitude 1.

The Boussinesq–Oberbeck equations are discretized by using a second-order backward Euler approximation for the diffusive terms and a second-order Adams–Bashforth extrapolation for the advective terms. This yields, at each time step, a GSP, coupled with an elliptic Helmholtz equation, for the temperature. This temperature equation is solved at first in such a way that the body-force term of the momentum equation can be calculated.

For the computation we used eight subdomains and the following mesh in each of them: $16 \times 16 \times 48$. The time-step was equal to 5×10^{-3}.

In Fig. 1, where the vertical velocity in the median plane $z = L_z/2$ at different times is visualized, one observes the transition of the solution with 10 rolls to a solution with 8 rolls for which the wave number is approximately the critical one. Moreover, it was observed that the 3D flow becomes quickly 2D, so that, despite the initial perturbation of the temperature field, no 3D instability occurs. Especially as in [25], the skewed varicose instability (see, e.g., [26]) was not observed, probably due to a too strong confinement of the flow. The only instability that occurs is thus the Eckhaus instability, which results from the interaction of two neighboring rolls, the wave numbers of which are greater and smaller than the critical wavenumber.

Remark. When using for the mode number $k = 0$ the interface condition $[\![\partial_{xx} v]\!]_n = 0$, one obtains the same convective flow, the relative differences between the extrema of the vertical velocity being at most $O(10^{-5})$.

The same behavior was obtained for 2D calculations, done on a T3E computer, independently of the number of subdomains: $N = \{2, 4, 6, 8, 10\}$. For the perturbation of the initial conductive temperature field we used

$$\epsilon = -10^{-3}\sin(\pi y)\cos\left(\frac{\pi x}{0.8}\right) \tag{96}$$

in order to induce 10 rolls in the cavity. For all the calculations the same transition from 10 rolls to 8 rolls was observed. The quasi-stationary vorticity fields obtained at time $t = 20$

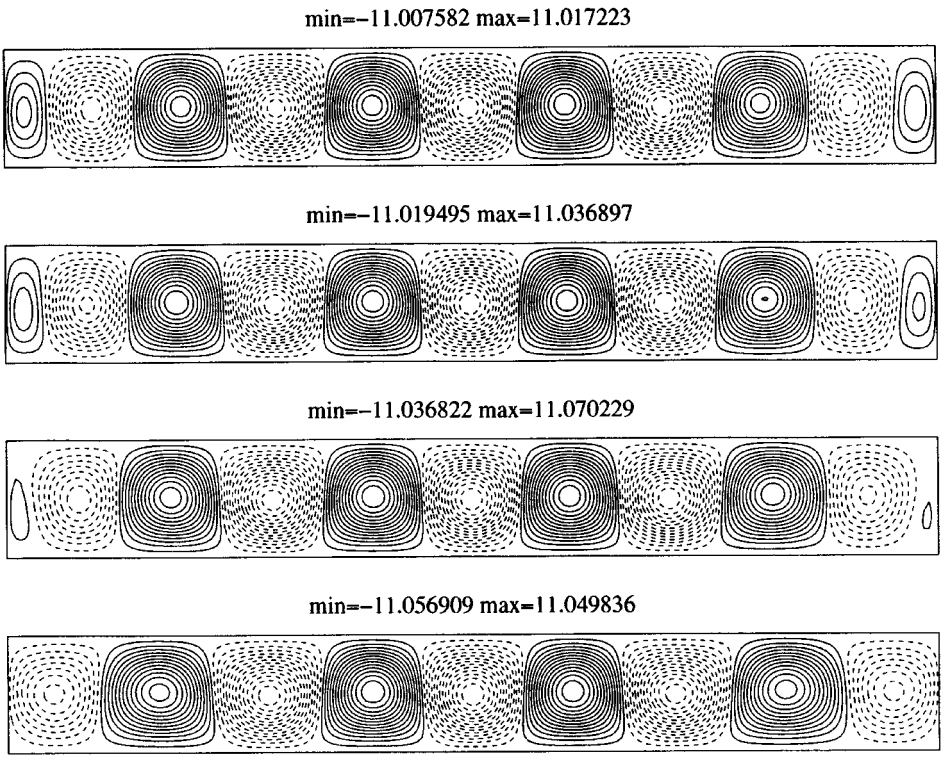

FIG. 1. Vertical velocity at times $t = 1.2$, $t = 1.6$, $t = 2$, and $t = 2.4$ (nondimensional values associated with the thermal diffusivity).

for the two extrema of the subdomain number are shown in Fig. 2. For all the considered values of N, the patterns are identical and the relative differences between the extrema of the vorticity are $O(10^{-6})$, after spectral interpolations on a unique regular grid. Moreover, the transition from 10 to 8 rolls agrees with the selection law obtained in [25], which indicates that for the present study the only stable patterns should show 7, 8, or 9 rolls.

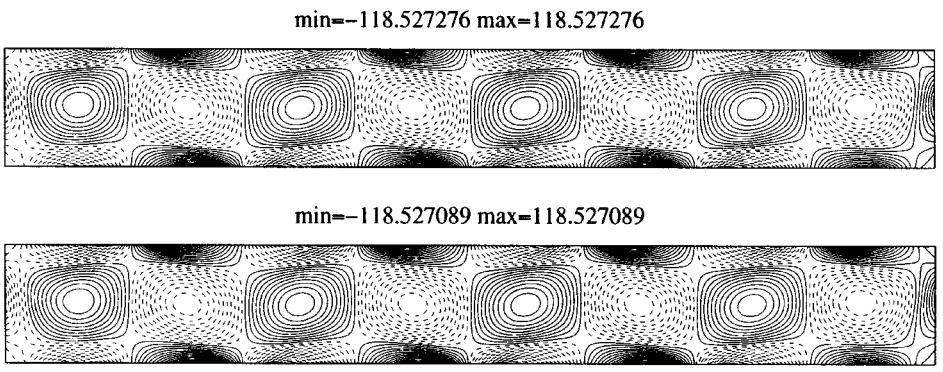

FIG. 2. Vorticity at time $t = 20$, computed with $N = 2$ and $N = 10$ subdomains.

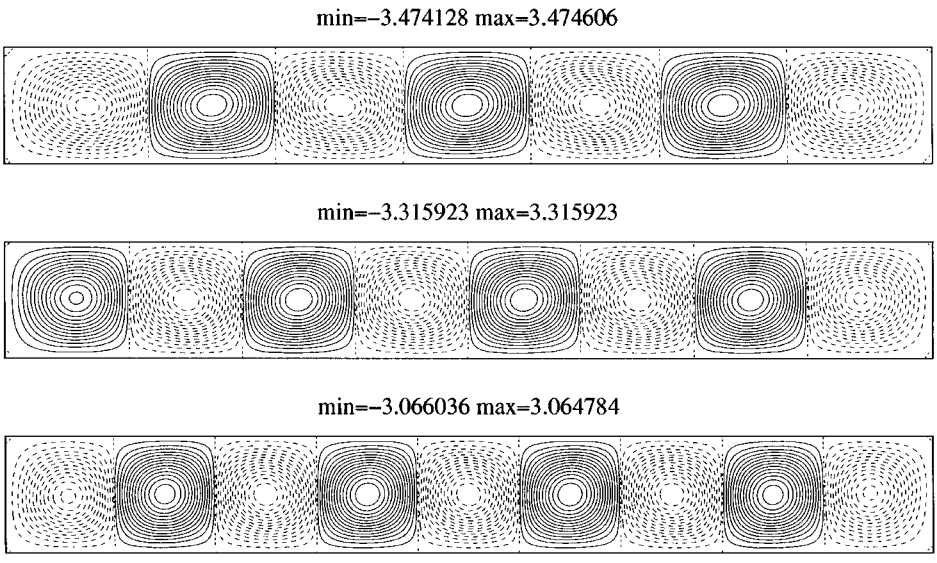

FIG. 3. Stream-function at time $t = 20$, for the three stable patterns.

It was interesting to check if the patterns with 7 and 9 rolls would be obtained with our multidomain solver. By changing the perturbation of the initial temperature field, these patterns have effectively been obtained. In order to get the 9 (or 7) roll configuration, we simply induced such flows by substituting in Eq. (96) the mean width of a roll to the 0.8 value. In Fig. 3 are shown the quasi-stationary stream-function, obtained at time $t = 20$, for the three stable configurations. When one iduces the 6 roll configuration, then one observes a transition yielding 8 rolls. Thus, for symetry reasons, the 6 and 10 roll configurations finally yield, with a gain or a loss of two rolls, exactly the same convective flow. For these calculations we used $N = 8$ subdomains.

Remark. In order to have an idea of the CPU time with respect to the number of subdomains, we give in Table 5 the CPU time needed by the most consuming processor for the preliminary calculations and for the simulation on the base of 1000 time steps. These results are not really favorable, since the total CPU time, i.e. when taking into account the number of processors, is nearly the same as $N \geq 4$ and even begins to increase for $N = 10$. Such poor results were expected for the test-case considered, which does not require many collocation points in each subdomain. In this situation, the CPU time needed by the computation of the interface velocity values, with exchanges of data between the different processors,

TABLE 5
CPU Time/Processor for the Preliminary Calculations and for 1000 Simulation Time Steps

N	2	4	6	8	10
Prel.	18.57	3.68	1.66	1.00	0.82
Sim.	62.86	22.26	14.46	10.66	9.34

is relatively important. This is no-more true when fine meshes are required, i.e. when the multidomain approach is fully justified.

5. CONCLUSION

We have presented a multidomain procedure for solving in 3D cartesian geometries of high aspect ratio with one homogeneous direction, the generalized Stokes problem (GSP) which results from the finite difference approximation of the incompressible Navier–Stokes equations. The main property of this Fourier–Chebychev spectral solver is that the discrete formulation of the GSP is exactly solved in such a way that the resulting velocity field is perfectly divergence-free. This is obtained in the following manner:

(i) in each subdomain, extended influence matrices are used to compute the boundary values of the pressure when taking into account that the equations are only enforced at the internal collocation points,

(ii) the velocity components at the interfaces of the different subdomains are computed by using block tridiagonal influence matrices, set up by using appropriate bases in order to enforce the compatibility conditions resulting from the incompressibility constraint.

Moreover, the problem of the spurious modes of pressure has been revisited and a new method has been proposed to recover the pressure field.

The computer code has been parallelized for a T3D (T3E) supercomputer and test results have been produced to outline that no drastic loss of accuracy occurs when the number of subdomains is increased as soon as the number of collocation points in each subdomain is sufficiently high. Finally, the capability of the code has been pointed out by solving a 3D Rayleigh–Bénard problem showing an Eckhaus instability and 2D numerical experiments have been achieved to demonstrate the credibility of the numerical results.

ACKNOWLEDGMENT

All the calculations have been performed on the CRAY T3D (T3E) computer of the IDRIS National Computational Center (91403 Orsay, France). Moreover, we thank J. M. Lacroix for his helpful technical support.

REFERENCES

1. H. C. Ku, R. S. Hirsh, and T. D. Taylor, A pseudospectral method for solution of the three-dimensional incompressible navier-stokes equations, *J. Comput. Phys.* **70**, 439 (1987).
2. G. E. Karnadiakis, M. Israeli, and S. A. Orszag, High order splitting methods for the incompressible navier-stokes equations. *J. Comput. Phys.* **97**, 415 (1991).
3. T. N. Phillips and G. W. Roberts, The treatment of spurious pressure modes in spectral incompressible flow calculations, *J. Comput. Phys.* **105**, 150 (1993).
4. O. Botella, On the solution of the navier-stokes equations using chebyshev projection schemes with third order accuracy in time, *Comput. & Fluids* **116**, 107 (1997).
5. A. Batoul, H. Khallouf, and G. Labrosse, Une méthode de résolution directe (pseudo-spectrale) du problème de stokes 2d/3d instationnaire. application à la cavité entrainée carrée. *C.R. Acad. Sci. Paris* **319**, (II), 1455 (1994).
6. M. Azaiez, A. Fikri, and G. Labrosse, A unique grid spectral solver of the nd cartesian unsteady stokes system, illustrative numerical results. *Finite Elements in Analysis and Design* **16**, 247 (1994).

7. P. Haldenwang and A. Garba, Pressure solvers of infinite order for 2d/3d generalized stokes problem, unpublished.
8. C. Canuto, M. Y. Hussaini, A. Quarteroni, and T. A. Zang, *Spectral Methods in Fluid Dynamics* (Springer-Verlag, Berlin, 1988).
9. L. Kleiser and U. Schumann, Treatment of incompressibility and boundary conditions in 3D numerical spectral simulations of plane channels flows, in *Proc. 3rd GAMM Conf. Numerical Methods in Fluid Mechanics, Notes on Numerical Fluid Mechanics*, Vol. 2 (Vieweg, Braunschweig, 1980), p. 165.
10. L. Tűckerman, Divergence-free velocity field in non periodic geometries, *J. Comput. Phys.* **80**, 403 (1989).
11. M. R. Schumack, W. W. Schultz, and J. P. Boyd, Spectral method solution of the stokes equations on non-staggered grids, *J. Comput. Phys.* **94**, 31 (1991).
12. G. Danabasoglu, S. Biringen, and C. L. Streett, Application of the spectral multidomain method to the navier-stokes equations, *J. Comput. Phys.* **113**, 155 (1994).
13. H. H. Yang and B. Shizgal, Chebyshev pseudospectral multi-domain technique for viscous flow calculation, *Comput. Methods Appl. Mech. Engrg.* **118**, 47 (1994).
14. M. Azaiez and A. Quarteroni, A spectral stokes solver in domain decomposition methods, *Contemp. Math.* **180**, 151 (1994).
15. W. Couzy and M. O. Deville, A fast schur complement method for the spectral element discretization of the incompressible navier-stokes equations, *J. Comput. Phys.* **116**, 135 (1995).
16. A. Quarteroni, Domain decomposition methods for the incompressible Navier–Stokes equations, in *ECCOMAS'94 Conference, Stuttgart, 1994*, edited by S. Wagner, E. H. Hirschel, J. Périaux, and R. Piva, p. 72.
17. J. P. Pulicani, A spectral multi-domain method for the solution of 1d helmholtz and stokes type equations, *Comput & Fluids* **16**(2), 207 (1988).
18. I. Raspo, J. Ouazzani, and R. Peyret, A direct chebyshev multidomain method for flow computation with application to rotating systems, *Contemp. Math.* **180**, 533 (1994).
19. I. Raspo, J. Ouazzani, and R. Peyret, A spectral multidomain technique for the computation of the czochralski melt configuration, *Int. J. Num. Meth. Heat Fluid Flow* **6**, 31 (1996).
20. P. Le Quéré and T. Alziary de Roquefort, Computation of natural convection in two-dimensional cavities with chebyshev polynomials, *J. Comput. Phys.* **57**, 210 (1985).
21. R. K. Madabhushi, S. Balachandar, and S. P. Vanka, A divergence-free chebyshev collocation procedure for incompressible flows with two nonperiodic directions, *J. Comput. Phys.* **105**, 199 (1993).
22. S. Balachandar and R. K. Madabhushi, Notes: Spurious modes in spectral collocation methods with two non-periodic directions, *J. Comput. Phys.* **113**, 151 (1994).
23. C. Bernardi and Y. Maday, *Approximations Spectrales de Problèmes aux Limites Elliptiques* (Springer-Verlag, Paris, 1991).
24. R. Peyret, The chebyshev multidomain approach to stiff problems in fluid mechanics, *Comput. Meth. Appl. Mech. Eng.* **81**, 129 (1990).
25. J. C. Mitais, P. Haldenwang, and G. Labrosse, Selection of 2D patterns near the threshold of the Rayleigh-Bénard convection, in *Proc. 8th Heat Transfer Int. Conf.*, edited by C. L. Tien, V. P. Carey, and J. K. Serrell, Vol. 4, Hemisphere publishing corporation (San Francisco, USA, 1986), p. 1545.
26. H. L. Swinney and J. P. Gollub, *Hydrodynamics Instabilities and the Transition to Turbulence* (Springer, Berlin Heidelberg, New York, 1981).